Astron. Astrophys. 345, 265–275 (1999)

ASTRONOMY AND ASTROPHYSICS

Dynamics of the solar granulation

VI. Time variation of the granular shear flow

A. Nesis, R. Hammer, M. Kiefer, H. Schleicher, M. Sigwarth, and J. Staiger

Kiepenheuer-Institut für Sonnenphysik, Schöneckstrasse 6, D-79104 Freiburg, Germany (nesis@kis.uni-freiburg.de)

Received 28 September 1998 / Accepted 13 January 1999

Abstract. Excellent spectrograms can yield observational insight in the dynamics of the solar surface not yet accessible to numerical simulations. We present results of the elaboration of a series of spectrograms taken at the center of the solar disk. Each of the spectrograms includes more than 250 granules, while the series covers a time of 12 min. Our main emphasis is to study the dynamics of the visible solar layers not only as a function of height but also as a function of time.

We investigated the temporal and spatial behavior of the turbulent concentration at the granular borders and its spreading-out into the intergranular space. In the deep photosphere, enhanced turbulence is concentrated predominantly near granular borders, while at higher layers the turbulence spreads out over the entire intergranular space. Remarkable is the decay of the turbulence with the height in the photosphere. There was no significant variation of the turbulence over the 12 min.

We also determined the rms turbulent pressure at the granulation layers near $\tau_{5000} = 1$. The average ratio of turbulent to gas pressure is of the order of 0.1; values of this size are also discussed in recent theoretical works. In order to take the intermittency into account, we traced the peak to peak variations of the turbulent velocity, which turn out to be $\approx 4\,\mathrm{km\,sec}^{-1}$. The corresponding ratio of turbulent to gas pressure may thus reach locally significant values up to about 0.3.

We did not find either a correlation or an anticorrelation between turbulence and convective flow, although the turbulence is presumably generated by granular shear flow. We suggest that the intermittent turbulence in the visible layers and the convective flow constitutes a dynamical system. This *turbulence–granulation*–dynamical system exhibits a cyclic behavior corresponding to the *dynamical* time of the granules, i.e. the growth and decay of their velocity profile.

The power spectra of the turbulent and granular velocity show a two-component character, which presumably reflects the action of two different processes determining the dynamics of the solar convective boundary layers and above.

Key words: Sun: photosphere – Sun: granulation

Send offprint requests to: A. Nesis

1. Introduction

The dynamics of the granulation manifests itself best in the continuous variation of the visible solar surface. Time series of spectrograms and filtergrams map the velocity fields associated with the granular and intergranular motions, whereas series of white light pictures illustrate the fragmentation of granules as well as their lateral motions. Substantial variations of the dynamics of the overshoot layers occur over the mean life time of a granule, especially when large granules emerge.

So far, time sequences of spectrograms were used to study the penetration of granular motions into the photosphere or to obtain a two dimensional map of the velocity field associated with the granulation. Espagnet et al. (1995) used a 16-min time series of two-dimensional *Multichannel Subtractive Double Pass* spectrograms, recorded in the NaD_2 5690 absorption line, to study the vertical structure of the photosphere and the penetration of granules. Johannesson (1992) applied an improved version of the imaging technique presented in Johannesson et al. (1992) to a field of quiet granulation. They used as observational material a scan containing 170 pairs of spectra and slit-jaw images. Bendlin & Volkmer (1995) and Salucci et al. (1994) analyzed series of filtergrams of the granular velocity field obtained with a narrow Fabry-Perot instrument. Espagnet et al. (1995) follow also the evolution of photospheric features in white light pictures as well as bright features ("plumes") of the upper photosphere.

In earlier papers of this series (e.g., Nesis et al. 1997) we investigated the dynamics of the granulation on the basis of a single excellent spectrogram carefully selected from a series of spectrograms of varying quality. In view of the "one-dimensionality" of our data, the qualitative agreement of the results of our investigations with those of the above mentioned publications is particularly remarkable.

The one-dimensional investigation of the granulation dynamics revealed the existence of a shear flow at the border of some granules which likely produces a turbulent velocity field located in the intergranular space. In this context the granular flow can be considered as a laminar flow extending up to more than a pressure scale height above the visible layers. At this point the question arises whether these results change over the granules life time or remain qualitatively the same.

In order to find out how the dynamics of the intergranular space changes with time, we extended our investigation to a series of spectrograms of comparable quality (see Nesis et al. 1997, 1998a, 1998b). The processing of the 7 best spectrograms from a series covering 12 min shows that the intergranular space is always turbulent, whereas granules reveal a practically purely laminar convective flow. In the deep photosphere, regions of enhanced turbulence in the intergranular space are concentrated predominantly near the granular border. At higher layers, however, the turbulence spreads out over the entire intergranular space. Remarkable is the decay of the turbulence with the height in the photosphere.

The importance of turbulence for the understanding of the dynamics of the solar granulation and thus of the physics of the upper convective layers has been increasingly recognized over the past few years and is well documented by the paper of Rosenthal et al. (1995). Rosenthal (1998) calculated the modification of the adiabatic exponent Γ_1 by the turbulent pressure, which can correct the discrepancy between measured mode frequencies and calculations for a standard solar model for a broad range of p-modes and f-modes. The influence of the turbulent pressure on models of the convective zone in connection to helioseismology was tested by Baturin et al. (1998). Nordlund et al. (1997) asked if stellar granulation is turbulence. Nordlund (1997) stressed the importance of the turbulent pressure in connection with the excitation and damping of the p-modes.

In the current investigation we address the role of turbulence and turbulent pressure from an observational point of view: we infer its height dependence and its relationship to the granular velocity. Furthermore we discuss the influence of the history of the granulation on the turbulence field of the upper layers of the convective zone.

2. Material and methods

2.1. Material

The observational material on which this study is based consists of photographic spectrograms taken with the German Vacuum Tower Telescope (VTT) in Izaña (Tenerife) in May 1994. A series of spectrograms was taken at the same position at the center of the solar disk every 15 sec, covering about 20 min in total. Of these spectrograms, 7 (94.A4, 94.A22, 94.A23, 94.A48, 94.A49, 94.A50, 94.A51) turned out to be of particular high quality and are therefore used in this study. (The quality of the spectra was judged both visually, on the basis of the crispness of line wiggles seen in a microscope, and numerically, based on the properties of power spectra.) They cover a time span of 12 min, corresponding approximately to a mean turn-over time of a granule (cf. Mehltretter 1978). The exposure time was 4 sec. The wavelength range was $\lambda\lambda$: 491.00 — 491.40 nm and included several absorption lines of different strength. The slit width was 60 μ. For a detailed description see Nesis et al. (1996, 1997).

With these absorption lines we could measure Doppler velocity as well as line broadening fluctuations *simultaneously* at different heights in the photosphere within the first 230 km above the continuum, whereas by means of the 7 spectrograms we trace the convective and turbulent field over the mean life of the granulation.

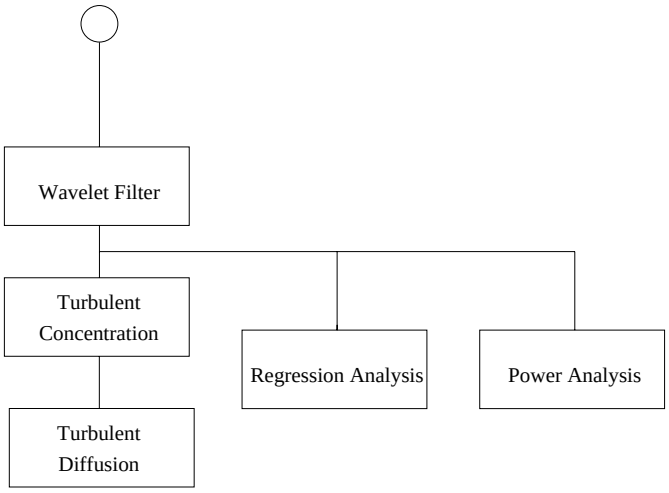

Fig. 1. Flow chart of the data processing steps

Both the Doppler velocity fluctuations $v_{\rm conv}$ and the line broadening fluctuations FWHM were measured along the spectrograph slit at equidistant positions s_i ($i = 0, 1, \cdots, 676$). The $v_{\rm conv}$ variations were measured as Doppler shift fluctuations of the line core, while the line broadening fluctuations FWHM correspond to the full line width at half maximum (cf. Nesis et al. 1993). Because the absorption lines are to first order magnetically and thermally insensitive and the line asymmetry is negligible, the FWHM reflects an unresolved photospheric velocity field w which unambiguously includes photospheric turbulent velocity fluctuations; thus in the following we will refer to $w_{\rm turb}$ as turbulent velocity as opposed to the granular convective velocity $v_{\rm conv}$. By calculating the line profiles we verified that the lines have a small temperature sensitivity, as expected for neutral metal lines of ca. 4 eV excitation energy.

2.2. Method

The data processing steps in the course of the data elaboration are shown in Fig. 1, their detailed description is given in the next paragraphs.

Wavelet filter. According to Meyer (1993) a wavelet transform presupposes the following necessities: The analyzing wavelet is required to have zero average, wavelets have to be continuous functions, and there should be a single, spatially localized 'mother function', which is 'translated' to cover all positions and 'dilated' to obtain the scale decomposition. Furthermore, a reconstruction formula has to exist for recovering the signal exactly from its wavelet coefficients. All analyzing wavelets are then mutually similar, and scale covariant with one another.

Wavelets can store separately the high and low frequency coefficients by the wavelet transformation (cf. Press et al. 1992). We use this property to remove the spatial high frequency noise.

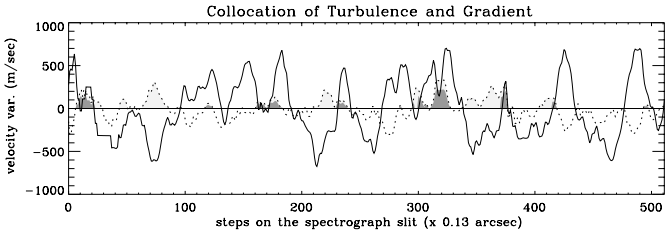

Fig. 2. The total variations of the convective velocity $v_{\rm conv}$ (full line) and the turbulence $w_{\rm turb}$ (dotted line) along the slit. The *grey color areas* mark the spots along the spectrograph slit with enhanced turbulence. Some of these spots are located at granular borders and coincide with large gradients of the convective flow (*dark color areas*).

The inverse wavelet transformation, in addition, enables us to control the filtering process in such a way that the original signal does not "suffer". The wavelets which we use in this paper are the orthogonal Daubechies functions which allow one to separate a signal into a minimal number of independent coefficients. They are defined on the so-called dyadic grid and are covariant by discrete translations and dilatations only (see Press et al. 1992). As a consequence, the length of the data in pixels has to be a power of two, and the resolved scales are also powers of two. Therefore, in the following figures we plot only 512 out of the 676 digitized data points along the spectrograph slit.

Concentration of the turbulence at granular borders and its spreading out into the intergranular space. Along the spectrograph slit the turbulence is distributed intermittently, in other words spottily. A trace of the turbulent velocity $w_{\rm turb}$ shows that *enhanced turbulence* $w_{\rm turb} > 0$ ($w_{\rm turb}$ represents the variation of the turbulent velocity with respect to its mean value which we define to be zero) is located in the intergranular space as well as at the borders of granules. These borders are also the places of strong horizontal gradients of the vertical granular flow, $\nabla v_{\rm conv}$, in other words of a shear flow, which is the locus where turbulence should be expected to be produced. We look, therefore, first for places where enhanced turbulence ($w_{\rm turb} > 0$; light gray areas in Fig. 2) and gradients of the granular upflow ($v_{\rm conv} > 0$) are co-located. The set of pixels where this collocation holds is thus given by the function $d = \nabla(v_{\rm conv} > 0) \wedge w_{\rm turb} > 0$, where the logical *and* operator $\wedge$ symbolizes the collocation.

A measure of the turbulence concentration at the granular borders is given by the correlation coefficient $c = d \otimes (w_{\rm turb} > 0)$, which correlates the points with enhanced turbulence with those that in addition are associated with velocity gradients in upflow regions. Thus c corresponds to the ratio of the total dark color area to the total gray color area in Fig. 2.

To quantify the spreading out of the turbulence $w_{\rm turb}$ into the intergranular space we calculate the coefficient β of the regression line $w_{\rm turb} = {\rm a} + \beta v_{\rm conv}$. Then only the case $\beta = 0$ infers an indifferent behavior of $w_{\rm turb}$ relative to $v_{\rm conv}$; any other value implies a tendency towards a correlation between these two velocities.

Regression analysis. We are interested in how the convective flow $v_{\rm conv}$ affects the turbulence state of the solar surface represented by the velocity $w_{\rm turb}$ and model this influence by a simple linear function $w_{\rm turb} = a_{\rm const} + \beta v_{\rm conv}$. To visualize better the behavior of the local *correlation* or *anticorrelation* between $v_{\rm conv}$ and $w_{\rm turb}$ on the solar surface we consider their difference $v_{\rm conv} - w_{\rm turb}$ as a function of the convective flow $v_{\rm conv}$ along the slit. The regression line in this case is $v_{\rm conv} - w_{\rm turb} = a_{\rm const} + \beta v_{\rm conv}$. According to the principle of ergodicity the spatial variation of the velocity difference $v_{\rm conv} - w_{\rm turb}$ reflects different states in the evolution of various granules or intergranular regimes with the time. In this context we speak of a phase difference $v_{\rm conv} - w_{\rm turb}$. The corresponding scatter plots represent the dynamical portrait of the *turbulence–granulation* dynamical system in their phase space over the 12 min observing sequence.

Power analysis. Observational data indicate that the turbulence in the granular overshoot layers is strongly associated with granular shear flow. Shear flow turbulence is anisotropic and its power spectrum is expected to follow a power law with an exponent different from the Kolmogorov exponent $-5/3$ for isotropic turbulence. Therefore, we also performed a power analysis of our data, similar to what we did in earlier papers (see Nesis et al. 1996). This time, however, we are considering turbulent variations; thus, the wave number k (and the associated length $\Lambda = 2\pi/k$) denotes the extension of turbulent spots in the granular layers.

Mean values of c, β and $< w_{\rm turb}^2 >^{1/2}$. For a better demonstration of the variation with height in the photosphere and to extrapolate to the granulation layers $\tau_{5000} = 1$, we average the quantities c, β and $< w_{\rm turb}^2 >^{1/2}$ over the 12 min time span of our observations. In doing so we are able to draw error bar lines. The calculation of mean values is justified because the above quantities show a qualitatively similar variation with height over the 12 min period.

3. Results

In the following we present our results ordered according to the data analysis flow chart in Fig. 1.

3.1. Concentration of turbulence at granular borders and its advection into the intergranular space

Fig. 2 shows the convective velocity $v_{\rm conv}$ (full line) and the turbulent velocity $w_{\rm turb}$ (dotted line) along the spectrograph slit; they are calculated on the basis of one (94.A4) of our spectrograms. The light gray areas are the positions along the slit with enhanced turbulence $w_{\rm turb} > 0$. The positions where such enhanced turbulence is co-located with gradients of the granular upflow $\nabla(v_{\rm conv} > 0)$ (see Sect. 2.2) are marked in dark gray. The intermittent character of the enhanced turbulence and its preference to be concentrated at granular borders are here clearly exemplified.

Table 1. Concentration of the turbulence at granular borders, c, and its "diffusion" into the intergranular space β. The seven spectrograms were taken at three different times (t= 1 min, 5.5 min, and 12 min after the start of spectrum 94.A4)

Height	t=1 min		t= 5.5 min				t=12 min							
	94.A4		94.A22		94.A23		94.A48		94.A49		94.A50		94.A51	
	c	β	c	β	c	β	c	β	c	β	c	β	c	β
70 km	0.77	0.11	0.61	0.20	0.61	0.15	0.79	-0.11	0.75	-0.11	0.74	0.02	0.74	-0.31
100 km	0.82	0.01	0.63	0.06	0.61	0.21	0.69	0.13	0.53	0.27	0.68	0.16	0.67	0.14
130 km	0.86	0.05	0.64	0.05	0.59	0.10	0.67	0.09	0.72	0.04	0.72	0.01	0.84	0.00
160 km	0.85	0.08	0.55	0.15	0.51	0.18	0.68	0.18	0.67	0.16	0.65	0.17	0.65	0.22
180 km	0.68	0.14	0.53	0.17	0.49	0.19	0.63	0.19	0.64	0.23	0.52	0.27	0.61	0.26
210 km	0.78	0.08	0.55	0.13	0.50	0.20	0.68	0.10	0.62	0.16	0.61	0.15	0.68	0.17

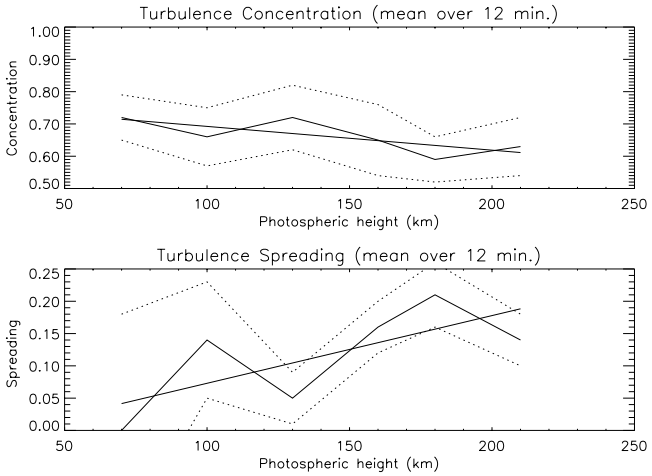

Fig. 3. Mean values of turbulent concentration c and spreading β averaged over all spectrograms. *Upper panel:* the degree of turbulence concentration to granular borders with large velocity gradient as a function of the height in the photosphere. *Lower panel:* the degree of turbulence spreading out into the intergranular space and its variation with height.

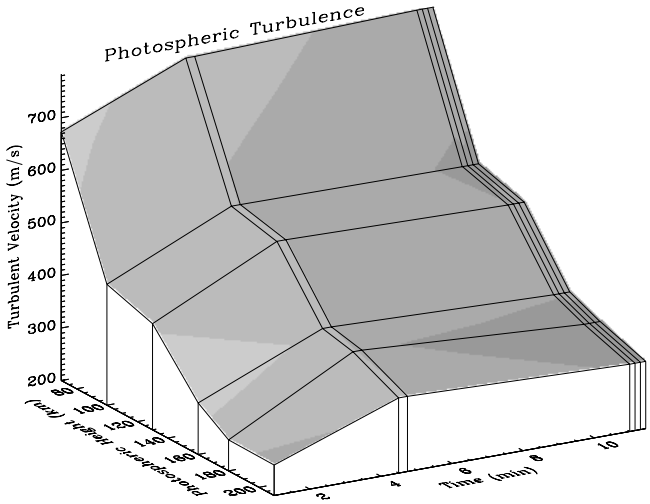

Fig. 4. The turbulent velocity as a function of time and height in the photosphere. First horizontal axis: height in the photosphere in km. Second horizontal axis: time in min. Vertical axis: rms values of the turbulence $< w^2_{\rm turb} >^{1/2}$. The vertical bars on the height axis mark the position where we have measured the turbulent variations $w_{\rm turb}$ whereas the bars on the time axis show the times at which we took the best spectrograms within the twelve minutes total period of our observations. (We do not analyze observations made at other time steps within this period since suboptimal seeing caused those data to be inferior.) In our analysis we average the two data points at 5.5 min and the four points near 12 min.

For each of the seven spectrograms we have calculated the turbulent concentration coefficient c as well as the turbulent spreading-out coefficient β (see Sect. 2.2). Table 1 shows the result of this calculation: the 7 columns each showing c and β, correspond to the 7 best spectrograms 94.A4, 94.A22, 94.A23, 94.A48, 94.A49, 94.A50, and 94.A51 out of the entire series that we analyze here. Because of the temporally fluctuating seeing conditions the time axis is not covered equidistantly, although spectrograms were taken every 15 sec (see Sect. 2.1).

The 6 rows correspond to the 6 different heights in the photosphere, which we can probe with our set of spectral lines, and which are shown in the first column. So, in Table 1 we can follow the variations of the concentration of enhanced turbulence c and its spreading-out coefficient β within the first 200 km above the granulation layer ($\tau_{5000} = 1$) over more than the mean turnover time of granules. However, a critical inspection of Table 1 reveals that c and β as functions of height in the photosphere exhibit qualitatively the same behavior in all 7 spectrograms; there is no significant discrepancy within the life time of a granule. Because of this behavior we averaged c and β over all spectrograms (12 min) by calculating the mean values $\overline{c}$ and $\overline{\beta}$ along the rows in Table 1.

Fig. 3 shows the mean values of c and β averaged over all seven spectrograms in Table 1, and the associated standard deviations. In the upper panel we see the variation of the mean concentration with height and its fit line (full line) which is embedded between the error-bar lines (dotted lines). The lower panel of Fig. 3 shows the spreading out of the turbulence and its variation with height as well as its fit line (full lines); both are embedded between the error-bar lines (dotted lines).

3.2. Turbulent velocity and turbulent pressure; their variation with time and height in the photospheric layers

Fig. 4 shows the rms turbulent velocity $< w^2_{\rm turb} >^{1/2}$ as a function of height in the photosphere (first horizontal axis) and time (second horizontal axis). The vertical lines on the height axis give the heights in the photosphere above the continuum

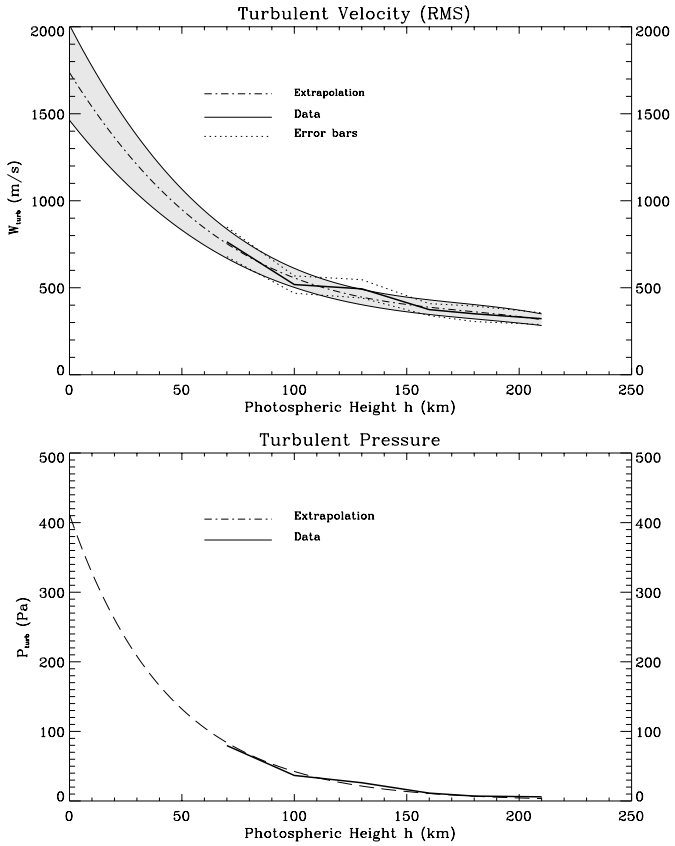

Fig. 5. Mean values $W_{\rm turb}$ of the rms turbulent velocities and the associated turbulent pressure averaged over all spectrograms. *Upper panel:* $W_{\rm turb}$ (strong full line) is the mean of the rms values $< w^2_{\rm turb} >^{1/2}$ with the error-bar lines (dotted) as functions of height. Both the rms values and their errors were fitted by polynomials and extrapolated to zero height (dash-dotted line and shaded area, respectively). The risk associated with this extrapolation is discussed in the main text (Sect. 3.2). The photospheric height zero corresponds to $\tau_{5000} = 1$. *Lower panel:* the pressure $P_{\rm turb}$ corresponding to the mean rms values $W_{\rm turb}$ (full line) and their extrapolation curve to zero height (dashed line).

(at $\tau_{5000} = 1$) where $< w^2_{\rm turb} >^{1/2}$ was calculated; the vertical lines on the time axis mark the times at which the seven selected spectrograms were taken. The time intervals between these spectrograms are not equal although spectrograms were taken every 15 sec (see Sect. 2.1), a consequence of the variable seeing conditions during the observation. As the time intervals between the spectrograms 94.A22, 94.A23 and 94.A48 to 94.A51, respectively, were very short, and the variations of the turbulent velocity very similar (within 5 to 13%, depending on height), we decided to replace the corresponding turbulent velocity by its mean value in Fig. 4. It is remarkable, however, that also the three different groups of spectrograms reveal a variation of $< w^2_{\rm turb} >^{1/2}$ with height which remains qualitatively the same over the turn-over time of a granule; therefore we calculated their temporal average denoted by an overline.

Figs. 5(upper panel) shows the averaged rms turbulent velocity $W_{\rm turb} = \overline{< w^2_{\rm turb} >^{1/2}}$ and its variation with the height in the photosphere(full line). The error-bar lines are also given(dotted lines). We fit the calculated rms turbulent velocity in the height interval 70 to 210 km by a polynomial function(dash-dotted line), which we used then to trace the rms turbulence velocity at the granular layers($\tau_{5000} = 1$). The same was done for the error-bar lines (shaded area) in order to estimate the uncertainty of the extrapolated mean value at zero height. (We are aware of the risk associated with this kind of extrapolation, but this is the best that can be done with the currently available data set. We are planning new observation campaigns to obtain data that sense the atmosphere at lower heights in order to reduce this uncertainty to some extent.)

Table 2. Hydrodynamical implications of our observations.

Re	ν_{turb}	P_{turb}	P_{turb}/P_{gas}	all values at
10^9	$10^8 m^2 s^{-1}$	$\leq 10^4$Pa	≤ 0.3	$\approx \tau_{5000} = 1$

The lower panel of Fig. 5 shows the turbulent pressure $P_{\rm turb}$ and its variation with height in the photosphere. $P_{\rm turb}$ is associated with the photospheric turbulent field and reflects the kinetic energy per volume $(1/2)\rho W^2$(see Hinze 1975). The atmospheric density ρ is taken from the atmosphere model of Vernazza et al. (1981). The turbulent pressure(full line) over the height interval 70 to 210 km is fitted very well by an exponential function. We used this function also to extrapolate the turbulent pressure down to the granulation layers. The exponential variation of the turbulent pressure $P_{\rm turb}$ reflects not only the run of the density ρ in the photospheric layers, but also the decay of the turbulent velocity $W_{\rm turb}$ with height. From our measurements we find that the latter decays with an exponential scale height of about 130 km, comparable to the scale height of the gas pressure in this part of the atmosphere according to the Vernazza et al. (1981) models, and somewhat smaller than the density scale height (150 km).

Table 2 shows the Reynolds number Re, the turbulent viscosity number $\nu_{\rm turb}$, a local maximum of the turbulent pressure $P_{\rm turb}$, and $P_{\rm turb}/P_{\rm gas}$; all these quantities refer to the turbulent velocity field at the granulation layers near $\tau_{5000} = 1$.

3.3. Phase space: turbulent velocity – convective velocity

The left column of Fig. 6 shows, in the four panels from the top to the bottom, the traces of turbulent(dotted lines) and convective velocity(full lines) of the spectrograms 94.A4, 94.A22, 94.A48 and 94.A50. The time span between the panel at the top(94.A4) and the one at the bottom(94.A50) amounts to 12 min, of the order of the turn-over time of granules. So, from the top panel down to the bottom one we follow the changes of the turbulence and the convective velocity over a typical granular life time; in other words we observe the history of the dynamics of the granulation. In the first panel the turbulent velocity $w_{\rm turb}$(dotted line) is smaller than in the other panels. In the third panel we see two large granules, a regular(step 30) and an exploding one(step 280). The emergence of the two large granules manifests the importance of considering the history of the dynamical behavior

of the granulation as will be discussed below, in connection with Fig. 6 right column, third panel from the top, regime 1.

The right column of Fig. 6 shows the scatter plots of the phase difference between convective flow and turbulence $v_{\rm conv} - w_{\rm turb}$ vs. the convective flow $v_{\rm conv}$ of the four selected spectrograms. The zero point of the $v_{\rm conv}$-axis and $v_{\rm conv} - w_{\rm turb}$-axis in the scatter plots is marked by a short vertical line. The diagonal $v_{\rm conv} - w_{\rm turb} = v_{\rm conv}$ marks the case of $w_{\rm turb} = 0$ i.e. the mean value of turbulence. The vertical dotted line through the zero point, and the diagonal divide the phase space in four regimes 1, 2, 3, and 4. The phase portrait in each of the four regimes reveals local aspects of the dynamics of the solar surface.

We realize, especially in the third panel from the top, that the phase difference between convective and turbulent flow $v_{\rm conv} - w_{\rm turb}$ varies in the regimes 1, 3 of each panel between positive and negative values. In regime 1 the positive phase difference reflects a local anticorrelation which we find within the granules: A convective upflow $v_{\rm conv} > 0$ associated with a reduced turbulence $w_{\rm turb} < 0$ (e.g. Fig. 6, left column, third and fourth panel, steps 30 and 290 along the slit, respectively). In regime 3 on the other hand the negative phase difference shows the dynamics which we observed in the intergranular space. We find again a local anticorrelation. Here, convective downflow $v_{\rm conv} < 0$ is associated with enhanced turbulence $w_{\rm turb} > 0$(e.g. left column third and fourth panel steps 40, 150, 310, 350 and 410 along the slit, respectively).

It is important to note that when we consider the entire slit we find no sign of a global correlation between convective flow and turbulence; the anticorrelation or correlation mentioned above refers to small parts of the velocity field along the spectrograph slit. So, the *turbulence–granulation*–dynamical system rather suggests a kind of "cyclic behavior". To visualize this behavior we use the terminology of predator–prey theories(see below) and assign population I to the convective flow and population II to the turbulence. In this sense growth and decay of population I represents the convective up- and downflow of granulation; whereas the enhanced and reduced turbulence is a manifestation of the growth and decay of population II. Positive phase difference in regime 1 reflects a maximum of population I associated with the decay of population II, while the opposite is the case in quadrant 3; here, the phase difference $v_{\rm conv} - w_{\rm turb}$ between convective and turbulence flow is negative. The pronounced shape of the phase portrait in regimes 1 and 3 of panel 3 coincides with the emergence of two particularly large convective upflows(bursts) associated with two granules, a regular and an exploding one; both of them generate turbulence. The time period of the *turbulence–granulation* system is tightly connected with the *dynamical* time of a granule. This is the time span corresponding to the growth and decay of the granular velocity profile.

3.4. Power spectrum of turbulence

Figs. 7 show the power spectra of the turbulence in the first 200 km above the granulation layers. The four panels correspond to the four spectrograms 94.A4, 94.A22, 94.A48, and 94.A50 and illustrate the granulation layers at different evolutionary times. The power spectra in the left column represent the dynamical situation within the first 100 km above the continuum($\tau_{5000} = 1$), whereas the power spectra in the right column represent the state of the turbulence in the layers well above 100 km. For the abscissa as well as for the ordinate we took a logarithmic scale. So we are able to recognize changes in the slope of the power distribution and to calculate quickly the exponent of a power law fit, which is an important characteristic of the physical processes that determine the power distribution.

In the right and left in Fig. 7 the short full line fits a slope of the power in the left column last panel from the top in the wave number range [1.15,1.4]. We have retained the same slope for all panels to demonstrate the possible variations of the power with the time and height in the photosphere. The dark area marks the behavior of the power within the wave number range [0.75,1.1]. In this range the power is quasi-constant and shows little variations with height and time.

4. Discussion

4.1. Concentration and spreading-out of the turbulence

As shown in Fig. 2 the turbulence is concentrated at the granular border and is mostly associated with large velocity gradients and thus with the granular shear flow. Table 1 shows the turbulent concentration c and the spreading-out of the turbulence β as functions of time(7 columns) and height in the photosphere(6 rows). A critical inspection of Table 1 reveals that c and β as functions of height exhibit qualitatively the same behavior. The mean values of c and β as functions of the height in the photosphere only(see Sect. 3.1) are shown in Fig. 3. In the upper panel of Fig. 3 we realize (i) that the mean turbulence concentration $\overline{c}$ is large in the deep photospheric layers and (ii) that $\overline{c}$ varies moderately with the height. The fact that $\overline{c}$ is large in the deep photosphere reflects the association of the turbulence with large gradients or strong shear flows(Nesis et al. 1997), whose moderate variation with the height(Nesis et al. 1997) causes the flat variation of $\overline{c}$. In the lower panel of Fig. 3 we realize (i) that the mean spreading-out of the photospheric turbulence $\overline{\beta}$ is small in the deep photospheric layers and (ii) that $\overline{\beta}$ varies drastically with the height in the photosphere. The variation of $\overline{\beta}$ and $\overline{c}$ reveals the change of the dynamical state of the intergranular space with height: In the deep photosphere the intergranular space is dominated by the granular downflow and partially by the turbulence located at the granular borders, whereas one pressure scale height higher the intergranular space is occupied by convective downflows as well as from turbulence. According to our findings above, the photospheric turbulence is spatially correlated with shear flows and might well represent *a shear turbulence* generated, deep in the photosphere, by the large gradients of the granular upflow. This raises the question if the granular shear flow might be also the source of significant pressure fluctuations.

It is obvious that shear turbulence generates pressure fluctuations. In particular the transition to turbulence in shear flow may

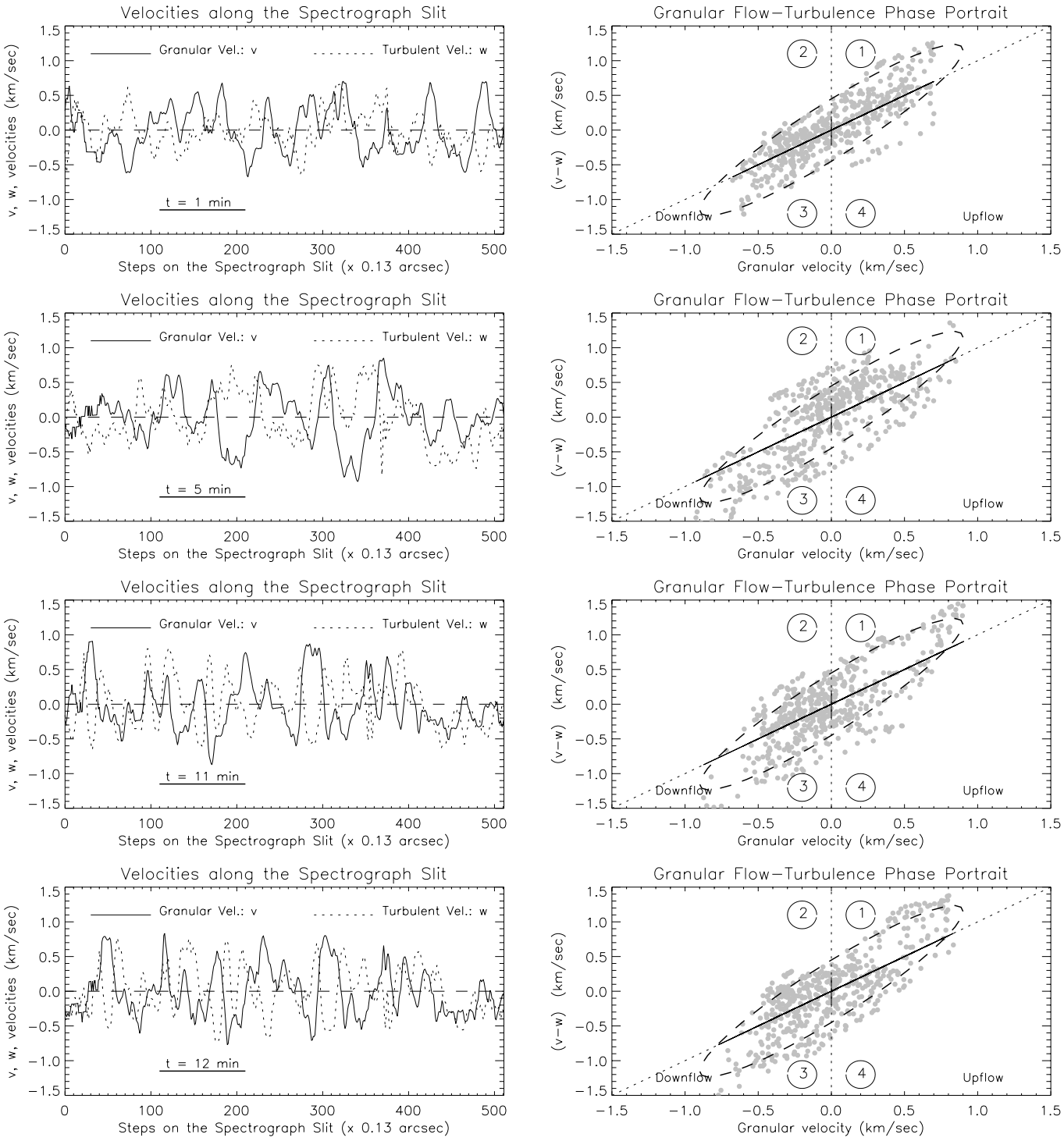

Fig. 6. *Left column:* Doppler velocity $v_{\rm conv}$(full line) and the turbulent velocity $w_{\rm turb}$(dotted line) along the spectrograph slit, taken at four different times at the same place on the solar disk.The four panels from the top of the page represent four different moments of the granulation within a total time span of 12 min. *Right column:* scatter plots of the difference $(v_{\rm conv} - w_{\rm turb})$ vs. $v_{\rm conv}$ of the velocities $v_{\rm conv}$ and $w_{\rm turb}$ shown in the corresponding left panel. The dashed line marks details of the scatter plots; the full line is the diagonal $v_{\rm conv} - w_{\rm turb} = v_{\rm conv}$ line. The vertical bar in the middle marks the zero point of the axes.

be accompanied by the generation of oscillations(see Schlichting 1982; Tritton 1991). Since according to our results shear flows and enhanced turbulence are predominantly located at granular borders, it is justified to expect that these are also the sites where stronger pressure fluctuations are generated. Hoekzema (1997) tried among others to localize the sources

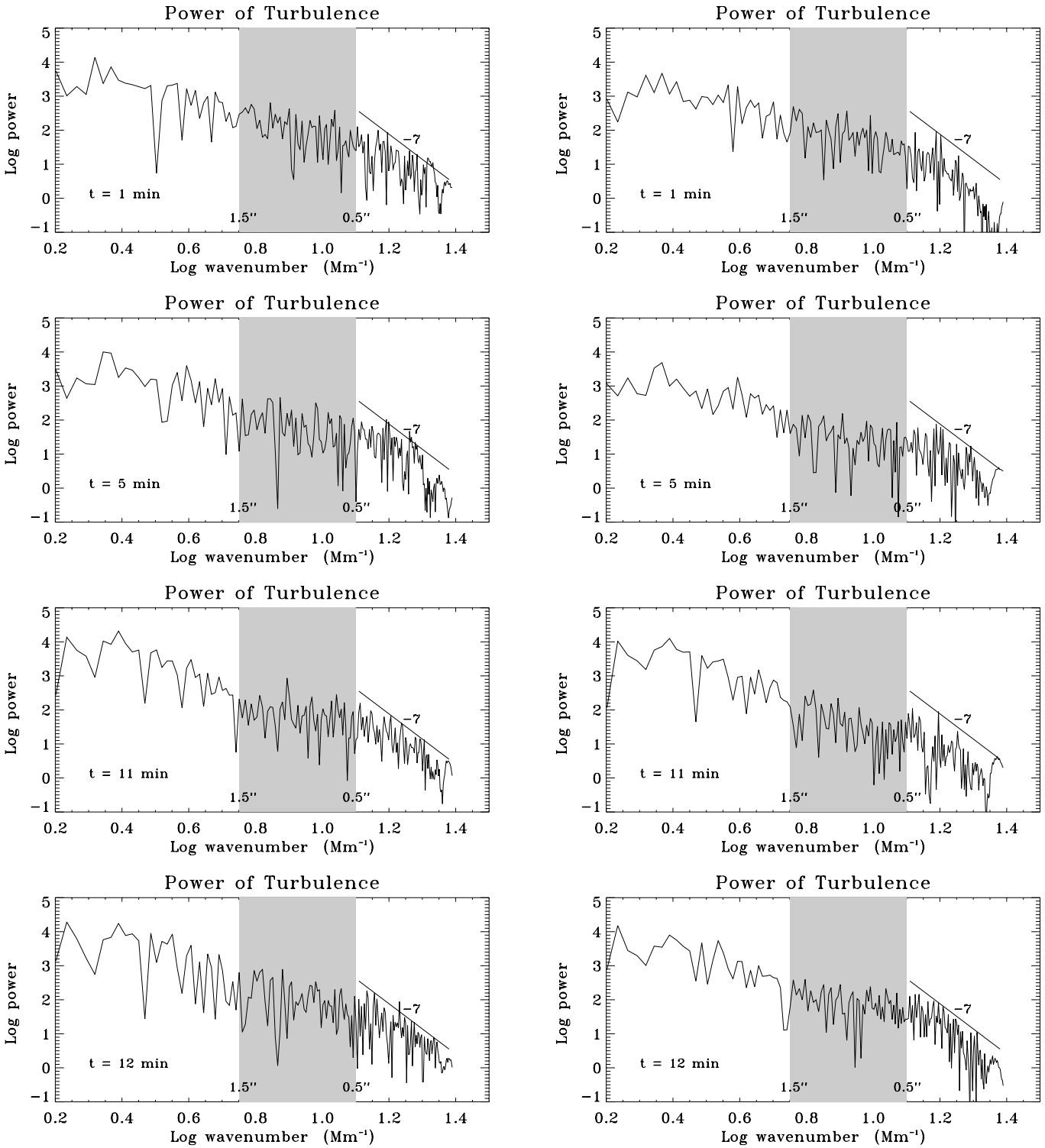

Fig. 7. *Left column:* Power spectrum of the turbulence(line broadening) $w_{\rm turb}$ calculated by means of two different absorption lines. *Left column:* $\lambda 491.25$ nm, formed ≈ 100 km above the continuum level. *Right column:* $\lambda 491.12$ mn, formed $\approx$ 170 km above the continuum level. We applied a filtering process based on wavelet techniques, which is most efficient for wavenumbers $\log k > 1.1 \mathrm{Mm}^{-1}$ (cf. Sect. 2.2).

of pressure oscillations in the photospheric layers. He reported high power above intergranular lanes and little power above granules and found that edges of granules might indeed act as sources of the 5 min oscillation, while he found no indication for excess acoustic emission near intergranular holes, as would be expected above downflow plumes.

Two-dimensional observations of line widths (FWHM) were performed by Johannesson (1992) and Bendlin (1993)

by means of different observational techniques: Johannesson (1992) scanned the image of a nonactive region of the Sun over the slit in order to provide a two-dimensional coverage. He found a fine network with reduced broadening which is co-spatial with intergranular lanes, and a few areas with strongly enhanced broadening that are also located in the intergranular lanes. The results of Johannesson (1992) are noteworthy here because they reveal the behavior of the line broadening at the higher photospheric layers; in contrast to our results, which concern the turbulence of deep photospheric layers. According to our Fig. 4 and earlier results(Nesis et al. 1997) the photospheric turbulence looses its amplitude and its coherence, respectively, with increasing height in the photosphere. Bendlin (1993) mapped the image of the sun by a two-dimensional Fabry-Perot interferometer; she found "smaller" profiles in granules and enhanced line broadening at all other places. These results reflect the dynamics of the deep photospheric layers. Salucci et al. (1994), using series of filtergrams obtained with a UBF and FP interferometer mounted in tandem, found the granular motion to be turbulent for heights larger than 170 km and convective at lower heights.

4.2. Turbulence and turbulent pressure

Fig. 4 shows the root mean square(rms) of the turbulent variations $< w_{\rm turb}^2 >^{1/2}$ as a function of time and the height in the photosphere. Remarkable is the fact that $< w_{\rm turb}^2 >^{1/2}$ does practically not vary with time, although it decreases steeply with height.

The upper panel of Fig. 5 shows the temporal mean of the rms values(presented in Fig. 4) $W_{\rm turb} = \overline{< w_{\rm turb}^2 >^{1/2}}$ as a function of height only(Sect. 3.2). Noteworthy is the large value of turbulence at $\tau_{5000} = 1$. The convective velocity $v_{\rm conv}$ is approximately half of the turbulent velocity(cf. Nesis & Mattig 1989).

The kinetic energy associated with the turbulence turns out to be an important factor in helioseismology investigations. The turbulent kinetic energy per volume, the turbulent pressure $\rm P_{turb}$, could affect the thickness of the strongly superadiabatic layers and thus some of the results of helioseismology(see Rosenthal 1998). According to Stein & Nordlund (1998), turbulent pressure is important in extending the mean atmosphere in the superadiabatic layers and above, which lowers the eigenfrequencies of medium and high ℓ modes whose upper turning points lie in this height range.

The lower panel of Fig. 5 shows the turbulent pressure associated with the temporal mean of the turbulence velocity, $P_{\rm turb} \propto \rho W_{\rm turb}^2$(see Fig. 5, upper panel) as a function of the height in the photosphere. Its extrapolated value at the continuum layers is of the order of 0.4×10^3 Pa, one order of magnitude less than the value of the gas pressure $\rm P_{gas} \approx 1 \times 10^4$ at these layers(see Vernazza et al. 1981). In these results, the turbulent velocity was determined from our observations.

We traced the peak to peak turbulent velocity variations $w_{\rm turb}$ along the slit (see e.g. Fig. 2) and found intermittently at the deepest photospheric layers peak to peak velocities $w_{\rm turb} \approx 4\,\rm km\,sec^{-1}$. The associated turbulent pressure $\rm P_{turb} = 0.2 \times 10^4$ Pa is no more negligible, and the quotient $\rm P_{turb}/P_{gas} \leq 0.3$ is considerable.

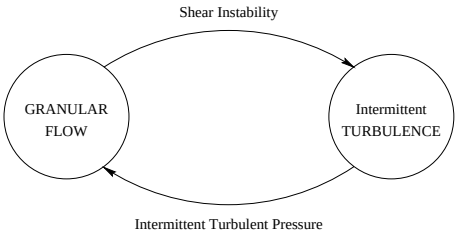

Fig. 8. This cartoon illustrates the working of the *turbulence-granulation* dynamical system: At locations of steep gradients in the granular flow patterns, shear instability produces turbulence. The associated turbulent pressure will backreact on the convective flow.

Table 2 shows some hydrodynamical implications of our results: the Reynolds number Re the turbulent viscosity $\nu_{\rm turb}$, and the local maximum values of the turbulent pressure $\rm P_{turb}$ as well as the ratio $\rm P_{turb}/P_{gas}$; all these quantities are associated with the turbulent velocity field at the granulation layers near $\tau_{5000} = 1$. An important parameter associated with the shear flow at the granular border is the Reynolds number $\rm Re = ul/\nu_{gas}$. According to our observations the convective velocity u is of the order of $10^5\,\rm cm\,sec^{-1}$, the characteristic thickness l of the shear flow of the order of 10^7 cm and the kinematic viscosity $\nu_{\rm gas}$ of the order of $10^3\,\rm cm^2\,sec^{-1}$(cf. Edmonds 1957). Thus the Reynolds number at $\tau_{5000} = 1$ is of the order of 10^9 (cf. Komm et al. 1991). It is well known that the turbulent velocity field changes the properties of the transport coefficients of the plasma. Here the turbulent viscosity $\nu_{\rm turb}$ is one important parameter, which can be determined by $\overline{\rm u_i u_j} = \nu_{\rm turb}(\partial \rm u_i/\partial x_j)$. Based on our observations we find that $\nu_{\rm turb} \approx 10^{12}\,\rm cm^2\,sec^{-1}$ at $\tau_{5000} = 1$; and the observed convective velocity $\rm u_i \approx 1\,km\,sec^{-1}$ at the granular border drops to zero over a length of 300 km parallel to the solar surface. The calculated turbulent viscosity $\nu_{\rm turb}$ is larger than the eddy viscosity $\nu_{\rm eddy}$ estimated by Bray & Loughhead (1967).

The dynamical pressure $\rm P_{turb}^{gran}$ associated with the flows in the granulation layers is proportional to $< v_{\rm tot}^2 >^{1/2}$ where $< v_{\rm tot}^2 >$ consists of both the line of sight and the horizontal granular velocity. Taking $\approx$1 km sec^{-1} for both components(Nesis & Mattig 1989) and a gas pressure $\rm P_{gas}$ typical of the granulation layers(see Stix 1989) the quotient $\rm P_{turb}/P_{gas} \leq 0.12$. This value has also been used in the theoretical works of Rosenthal et al. (1995) and Stein & Nordlund (1998).

4.3. Turbulence-granulation dynamical system

The fact that turbulent spots are found predominantly at granular borders suggests the existence of an intrinsic relationship between turbulence and granulation. To probe the nature of this relationship as well as its behavior with time we made use of a scatter plot $(v_{\rm conv}, w_{\rm turb})$. This scatter plot represents the portrait of the *turbulence–granulation* dynamical system in the $(v_{\rm conv}, w_{\rm turb})$ phase space.

The four panels in the right column of Fig. 6 show the changes of the state of the dynamical system(granulation) due to the mutual influence of turbulence and granular flow over the life time of a granule. These changes are tightly connected with the variations of the convective flow and the associated turbulence as well as with the emergence of large granules, as is shown in the left column of Fig. 6 especially in third and fourth panel.

When we compare the phase space plots(right column) from the top to the bottom of Fig. 6 we realize the following: in the top panel the points $(v_{\rm conv}, v_{\rm conv} - w_{\rm turb})$ are clustered more or less inside the ellipse(dashed line). This is obviously due to the small values of the turbulent velocity $w_{\rm turb}$(see the dotted line in the left column of Fig. 6, top panel). In the third panel from the top we have points in the extreme upper right corner above the diagonal which follow the line of the ellipse. This is because at that time(cf. left column of Fig. 6, third panel), two large granules can be seen at steps 30 and 290 along the slit, respectively. Furthermore we have also points in the extreme lower left corner below the diagonal outside of, but following the shape of the ellipse. These points reflect the enhanced turbulence in the intergranular space that can be seen at steps 40, 150, 310, 350 and 410. In the lowermost phase space plot this behavior begins to disappear as the large granules become less prominent when the convective velocity decreases.

Noteworthy is the change of the dynamics of the solar surface due to the emergence of the two large granules. As a result of this event the phase portrait seems to reveal a process cycle of the turbulence-granulation dynamical system which intersects the four parts of the panel. During this cycle large convective upflows associated with *reduced* turbulence (1) alternate with large downflows associated with *enhanced* turbulence (3). In other words turbulence generation by shear flows alternate with the turbulence decay due to diffusion and spreading with the height. If the ergodicity principle is applicable any physical state found along the slit is realized in time at a single point. In this sense in the third panel from the top the phase portrait reflects the periodical cycle of the turbulence-granulation dynamical system: large convective flow with small turbulence followed by large turbulence in the intergranular space, where the convective flow is small.

A theoretical model explaining this kind of behavior is the predator-prey model as described by the Volterra-Lotka equations (cf. Hirsch & Smale 1974). We assert that the feedback coefficient needed for the cyclic behavior of the system is the intermittent turbulent pressure $\mathrm{P_{turb}}$, which controls not only the pressure scale height in the visible layers but also the adiabatic exponent Γ_1 and the energy transfer in the super-adiabatic convective layers. The behavior of the large intermittent turbulence of the visible layers is tightly connected with the history of the dynamics of these layers. The emergence of a regular and exploding granule as well as their decay is associated with strong shear flows and thus with the production of turbulence. In other words turbulence is produced as long as shear flows exist at the granular borders i.e. within the time interval of growth and decay of a large granule within its *dynamical* time.

In the left column of Fig. 6 we recognize that the dynamics of the solar surface changes noticeably with time. Not only the amplitudes of the turbulent and convective velocity change but also the structuring of the velocity fields. The emergence and decline of the large granules near steps 30 and 300 along the slit of the lowermost two rows is reflected in the corresponding phase spaces by the change of the attractor-like shape. We like to notice that the spectrograph slit observed at all times the same place on the solar surface.

4.4. Power spectra

Figs. 7 show the power spectra of the turbulence at different times within the observing period of 12 min. The left column reflects the turbulence of the layers below one pressure scale height whereas the right column corresponds to layers above. The position of the power spectra relative to the slope line demonstrates the change of the power with height because the line remains at the same position. An important characteristic is the fact that the power function in the dark area remains constant. This implies a power law with an exponent near zero. This part of the power spectra, however, can result from the sum of descending and ascending power functions outside the dark area. This inference means that the turbulence power spectra are a composite of two individual components with their maxima at different positions on the horizontal axis. Such a behavior is typical for a transfer of energy: The power distribution at short wave numbers supplies energy to the system with the power at large wave numbers. This scenario supports the multifractal structure of the turbulence (see Frisch 1995).

5. Conclusions

Our observational material probes the behavior of the turbulence of the deep photospheric layers over 12 min. It reveals that in the deep photospheric layers the enhanced turbulence is predominantly concentrated at the granular borders, where it is presumably generated by strong granular shear flows. We found that with increasing height the turbulence attenuates and spreads out into the intergranular space; this behavior remained practically the same over the 12 min observing time.

The importance of the turbulent pressure $\mathrm{P_{turb}}$ for the super-adiabatic, convective boundary layers and above is obvious. Based on the rms turbulent velocity at $\tau_{5000} = 1$ we calculated the associated turbulence pressure $\mathrm{P_{turb}}$. We found for the ratio $\mathrm{P_{turb}/P_{gas}}$ at these layers an average value of ≈ 0.1, with local enhancements up to 0.3 at sites of large gradients. These results may serve as constraints for theoretical investigations. The behavior of the strongly intermittent turbulence of the visible layers is tightly connected with the history of the dynamics. The emergence and decline of both regular and exploding granules is associated with strong shear flows which could well be responsible for the production of turbulence. If this is the case, turbulence is produced as long as shear flows exist at the granular borders, i.e. within the dynamical time interval of the growth and decay of large granules.

Our data show the lack of any correlation or anticorrelation between the turbulence and the convective upflow in the photospheric layers. Turbulence and convective flow can rather be interpreted as a *turbulence–granulation* dynamical system with a cyclic behavior reflected the growth and decay of the granular velocity profile within its dynamical time.

We also calculated the power spectra of the turbulence velocity. The specific form of the power function, which does not change with time and height in the photosphere, can be understood in terms of two separate sources of power with maxima at different positions along the wave number axis. One of these power sources may supply energy to the other. This two-component form could be related to the granular turbulence dynamical system.

Acknowledgements. We are grateful to A. Brandenburg and A. van Ballegooijen for helpful discussions and to the referee, T. Foglizzo, for his constructive criticism.

References

Baturin V.A., Mironova I.V., Ayukov S.V., 1998, The Convection Zone and Oscillations. In: Deubner F.-L., Christensen-Dalsgaard J., Kurtz D. (eds.) Proc. IAU Symp. 185, New Eyes to See Inside the Sun and Stars. Kluwer Acad. Publ., p. 85

Bendlin C., Volkmer R., 1995, A&AS 112, 371

Bendlin C., 1993, Hochauflösende zweidimensionale Spektroskopie der solaren Granulation mit einem Fabry-Perot-Interferometer. Dissertation Univ. Göttingen

Bray R.J., Loughhead R.E., 1967, The Solar Granulation. Chapman and Hall LTD, p. 73

Edmonds F.N., 1957, ApJ 125, 535

Espagnet O., Muller R., Roudier Th., Mein P., Mein N., 1995, A&AS 109, 79

Frisch U., 1995, Turbulence. Cambridge University Press, p. 144

Hinze J.O., 1975, Turbulence. McGraw-Hill, 2nd ed., p. 24

Hirsch M.W., Smale S., 1974, Differential Equations, Dynamical Systems, and Linear Algebra. Academic Press, New York, p. 255

Hoekzema N., 1997, Statistical Studies of Dynamical Structures in the Quiet Solar Atmosphere. Proefschrift, Univ. Utrecht

Johannesson A., 1992, Observing with the Swedish Vacuum Solar Telescope La Palma, Lund Observatory Report

Johannesson A., Bida T.A., Lites B.W., Scharmer G.B., 1992, A&A 258, 572–582

Komm R., Mattig W., Nesis A., 1991 A&A 252, 812

Mehltretter P., 1978, A&A 62, 3

Meyer Y., 1993, Wavelets, Algorithms and Applications. Soc. for Industrial and Applied Math., Philadelphia

Nesis A., Mattig W., 1989, A&A 221, 130

Nesis A., Hanslmeier A., Hammer R., et al., 1993, A&A 279, 599

Nesis A., Hammer R., Hanslmeier A., et al., 1996, A&A 310, 973

Nesis A., Hammer R., Hanslmeier A., et al., 1997, A&A 326, 851

Nesis A., Hammer R., Kiefer M., Schleicher H., 1998a, The Solar Intergranular Space: Time and Height Variability. In: Donahue R.A., Bookbinder J.A. (eds.) Proc. 10th Cambridge Workshop on Cool Stars, Stellar Systems, and the Sun. ASP Conf. Ser. Vol. 154, p. CD-658

Nesis A., Hammer R., Kiefer M., Schleicher H., 1998b, Dynamics of the Deep Solar Photosphere at Subgranular Scales. In: Deubner F.-L., Christensen-Dalsgaard J., Kurtz D. (eds.) Proc. IAU Symp. 185, New Eyes to See Inside the Sun and Stars. Kluwer Acad. Publ., p. 451

Nordlund A., 1997, Excitation and Damping of P-Modes.In: Deubner F.-L., Christensen-Dalsgaard J., Kurtz D. (eds.) Proc. IAU Symp. 185, New Eyes to See Inside the Sun and Stars. Kluwer Acad. Publ., p. 199

Nordlund A., Spruit H.C., Ludwig H.-G., Trampedach R., 1997, A&A 328, 229

Press W.H., Flannery B.P., Teukolsky S.A., Vetterling W.T., 1992, Numerical Recipes, 2nd ed., Cambridge Univ. Press

Rosenthal C.S., 1998, Evidence for a Shallow Superadiabatic Layer. In: Provost J., Schmider F.-X. (eds.) Proc. IAU Symp. 181, Sounding Solar and Stellar Interiors. Poster Volume, p. 121

Rosenthal C.S., Christensen-Dalsgaard J., Nordlund A., Trampedach R., 1995, Convective perturbations to Solar Oscillations: the f Mode. In: Hoekzema J.T., Domingo V., Fleck B., Battrick B. (eds.) Proc. 4th SOHO Workshop, Helioseismology. ESA SP-376, Vol 2, p. 453

Salucci G., Bertello L., Cavallini F., Ceppatelli G., Righini A., 1994, A&A 285, 322

Schlichting H., 1982, Grenzschicht-Theorie. Verlag G. Braun Karlsruhe, p. 491

Stein R., Nordlund Å., 1998, ApJ 499, 914

Stix M., 1989, The Sun. Springer-Verlag, p. 145

Tritton, D.J., 1991, Physical Fluid Dynamics, 2nd ed., Oxford Sci. Publ. Clarendon Press Oxford, p. 279

Vernazza J.E., Avrett E.H., Loeser R., 1981, ApJS 45, 635